Regional Flow and Deformation Analysis of Basin-Fill Aquifer Systems Using Stress-Dependent Parameters

by Giona Preisig[1], Fabien Joel Cornaton[2], and Pierre Perrochet[3]

Abstract

Changes in effective stress due to water pressure variations modify the intrinsic hydrodynamic properties of aquifers and aquitards. Overexploited groundwater systems, such as basins with heavy pumping, are subject to nonrecoverable modifications. This results in loss of permeability, porosity, and specific storage due to system consolidation. This paper presents (1) the analytical development of model functions relating effective stress to hydrodynamic parameters for aquifers and aquitards constituted of unconsolidated granular sediments, and (2) a modeling approach for the analysis of aquifer systems affected by effective stress variations, taking into account the aforementioned dependency. The stress-dependent functions were fit to laboratory data, and used in the suggested modeling approach. Based on only few unknowns, this approach is computationally simple, efficiently captures the hydromechanical processes that are active in regional aquifer systems under stress, and readily provides an estimate of their consolidation.

Introduction

Hydrodynamic parameters, such as hydraulic conductivity, porosity, and specific storage, depend on effective stress (Louis 1969; Helm 1976; Gangi 1978; Walsh 1981; Kim and Parizek 1999; Rutqvist and Stephansson 2003; Galloway and Burbey 2011). However, governing equations used for regional analysis of aquifer systems, in general consider hydrodynamic parameters as stress-independent constants (Detournay and Cheng 1993; Murdoch and Germanovich 2006). This assumption is acceptable for shallow aquifers and for incompressible lithologies. However, there can be significant change in hydrodynamic parameters in deep and confined units subject to consolidation.

As defined by Terzaghi (1923) and Terzaghi and Peck (1967), effective stress describes the stress state of a saturated porous rock, and results from the load of principal stress on contacting grains and from water pressure in voids, which bears a part of the load (Bundschuh and Arriaga 2010). An increase of effective stress can result from (1) an increase of principal stress or (2) a decrease in water pressure. Both can lead to a reduction in porosity, and consequently in hydraulic conductivity and specific storage. These relationships are of an exponential type (Detournay and Cheng 1993), and for coarse-grained aquifers these are reversible only in the case of elastic small strains (voids closure/opening; Bell et al. 2008; Hansmann et al. 2012).

In earth sciences, many processes relate to changes in effective stress and hydrodynamic parameters. In hydrogeology, the decrease of hydraulic head due to groundwater pumping results in porosity reduction in aquifers and aquitards and causes land subsidence (Jacob 1940, 1950; Helm 1972; Holzer 1984; Gambolati et al. 2005; Galloway and Burbey 2011), as well as a reduction in well

[1]Corresponding author: Centre for Hydrogeology and Geothermics, University of Neuchâtel, Emile-Argand 11, 2000 Neuchâtel, Switzerland; giona.preisig@unine.ch

[2] DHI-WASY GmbH, FeFlow Scientific Development, Waltersdorfer Straße 105, 12526 Berlin, Germany.

[3]Centre for Hydrogeology and Geothermics, University of Neuchâtel, Emile-Argand 11, 2000 Neuchâtel, Switzerland.

productivity due to the decrease in reservoir permeability with the compaction. This last consequence is well known in petroleum engineering (National Research Council 1996). In geological engineering, the drilling of tunnels through porous units causes, among other responses, ground settlement (Lombardi 1988; Zangerl et al. 2003). On the other hand, ground uplift is recorded in areas subjected to fluid injection for geothermal energy production or CO_2 sequestration (Rutqvist et al. 2002; Ferronato et al. 2010). Finally, proposals regions for geologic radioactive waste repositories must be aware of such processes, which in the long term, can lead to brittle deformation.

For granular porous media, model functions relating effective stress to hydrodynamic parameters can be developed from two main theoretical approaches: (1) functions based on the size changes of solid grains (Hertzian theory of deformation of spheres; Gangi 1978) and (2) functions based on volumetric deformation of the bulk volume, that is, grains and voids (Kim and Parizek 1999). The deformation resulting from the change of the bulk volume is substantially greater than that derived from the compression of grains (Kim and Parizek 1999).

Two main methods are used for the analysis of groundwater flow in a deformable aquifer system: (1) nonsimultaneous analysis between groundwater flow (water pressures) and aquifer deformation (e.g., Jacob's approach 1940, 1950) and (2) simultaneous analysis (e.g., Biot's poroelastic theory 1941). Both approaches generally consider hydrodynamic parameters, in particular hydraulic conductivity and specific storage, as constants (Detournay and Cheng 1993; Murdoch and Germanovich 2006). In Jacob's approach, groundwater flow and deformation equations are partially coupled via the specific storage coefficient. In Biot's poroelasticity theory, equations are fully coupled via the volumetric strain that allows detailed simultaneous investigation of groundwater flow in a three-dimensional (3D) deformable porous medium. However, the complexity of the governing equations and the large number of unknown parameters limits its use to local scales and simple geological geometries (Kim 2005; Kihm et al. 2007; Galloway and Burbey 2011). For a detailed review of the analysis and simulation of groundwater flow in deformable aquifer systems, see Gambolati et al. (2005), Verruijt (2008), and Galloway and Burbey (2011).

Regional simulation of coupled hydromechanical processes considering detailed geological structures typically requires simplification of governing algorithms. The aim of this paper is to present a computationally simple approach for investigating coupled fluid-to-solid hydromechanical processes at a regional scale, with geologically oriented 3D meshes, considering the dependency of hydrodynamic parameters on effective stress.

The paper is organized as follows. First, the main hydrodynamic parameters (hydraulic conductivity, porosity, and specific storage) are linked to effective stress by means of analytical development. Then, a modeling approach based on few unknown parameters is presented and verified by a comparison with the Biot's poroelasticity theory.

A companion paper will focus on regional simulation of the Mexico City basin using the approach discussed herein. Note that, in this work, the terms consolidation and compaction are treated as synonyms and express the reduction in porosity and vertical aquifer thickness due to an increase in effective stress.

Effective Stress–Dependent Equations in Granular Porous Media

Granular porous media are formed of fine (clays and silts) and coarse (sand and gravel) grained materials. Aquifers are composed mainly of coarse-grained materials, while aquitards are composed of silts and clays (Figure 1a). A quaternary sedimentary basin is filled by spatial and temporal succession (sequential stratigraphy) and consists of several aquifers separated by areally extensive aquitards (Helm 1975). In both aquifers and aquitards, groundwater flow is Darcian. However, as described by Helm (1975), in aquitards groundwater flow is primarily vertical and very slow compared with the flow in aquifers. In such a case, aquitards can be conceptualized as doubly draining units. In this work, the term "aquifer system" refers to the vertical and horizontal succession of aquifers, aquitards, and confining units.

For elastic small strains, coarse-grained aquifers can be treated as Hookean materials (Jacob 1940, 1950). In Hookean materials, the change in porosity, hydraulic conductivity, and specific storage caused by increasing or decreasing effective stresses is reversible (elastic). Conversely, fine-grained materials are subject to nonreversible deformations, and when consolidated, only a portion of the loss in porosity is recoverable (Helm 1975; Galloway and Burbey 2011). Thus, two or more different model functions have to be used to reproduce one or more cycles of compression/expansion due to changes in applied effective stresses.

At the regional scale, land subsidence results from the complex and differential consolidation (in terms of time and location) of aquifers and aquitards constituting the aquifer system (Galloway and Burbey 2011) (Figure 1b).

In sedimentary basins and in the absence of tectonic stresses, the principal stress is the vertical component of the total stress tensor: $\sigma_v = \sigma_{zz}$. This corresponds to the weight of the overburden and increases with depth Z. The compression of sediments under the vertical stress induces horizontal stresses of equal magnitude $\sigma_h = \sigma_{xx} = \sigma_{yy}$ (Parriaux 2006; Price and de Freitas 2009). Under these conditions, the effective stress tensor $\boldsymbol{\sigma}'$ is expressed as:

$$\boldsymbol{\sigma}' = \boldsymbol{\sigma} - \alpha_{\mathbf{B}}\, p$$

$$\boldsymbol{\sigma}' = \begin{bmatrix} \sigma'_{xx} & \sigma'_{xy} & \sigma'_{xz} \\ \sigma'_{yx} & \sigma'_{yy} & \sigma'_{yz} \\ \sigma'_{zx} & \sigma'_{zy} & \sigma'_{zz} \end{bmatrix} = \begin{bmatrix} \lambda\sigma_{xx} & \sigma_{xy} & \sigma_{xz} \\ \sigma_{yx} & \lambda\sigma_{yy} & \sigma_{yz} \\ \sigma_{zx} & \sigma_{zy} & \sigma_{zz} \end{bmatrix} - \begin{bmatrix} \alpha_b & 0 & 0 \\ 0 & \alpha_b & 0 \\ 0 & 0 & \alpha_b \end{bmatrix} \rho_w\, g\, h \tag{1}$$

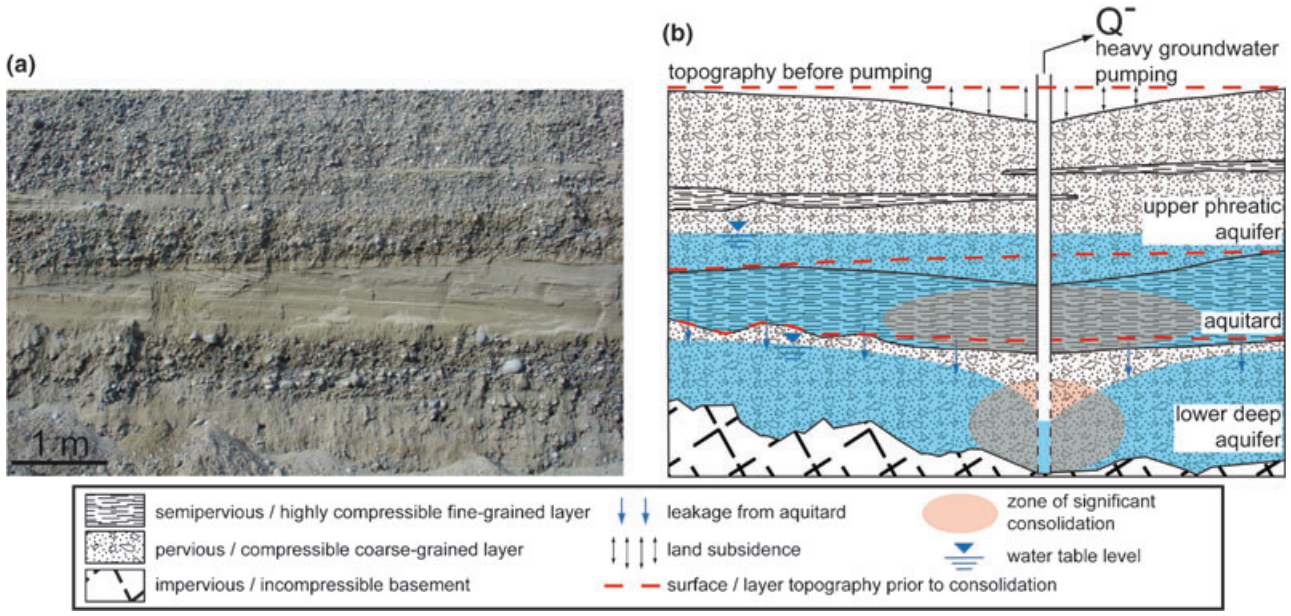

Figure 1. (a) Picture showing a sedimentary quaternary sequence of two coarse-grained strata, separated and interbedded by fine-grained layers (Seeland aquifer system, Switzerland). (b) Illustrative section, based on the left-picture, showing a regional aquifer system affected by land subsidence because of the consolidation of both (1) a leaking aquitard and (2) a heavily pumped aquifer.

where $\boldsymbol{\sigma}$ and $\boldsymbol{\alpha_B}$ are the total stress and the Biot-Willis coefficient tensors, respectively, p is water pressure, ρ_w is water density, g is gravitational acceleration, h is pressure head, and λ expresses the ratio of horizontal to vertical stress: $\lambda = \sigma_h/\sigma_v$. The Biot-Willis coefficient expresses the ratio of pore volume change to total bulk volume change: if there are no pores, then $\alpha_B \approx 0$, and if the total bulk volume change depends only on pore volume change, then $\alpha_B \approx 1$ (Bundschuh and Arriaga 2010). From Equation 1, it follows that the effective shear stresses, nondiagonal terms of $\boldsymbol{\sigma}'$, correspond to those of the stress tensor $\boldsymbol{\sigma}$, because water cannot support shear stresses (Galloway and Burbey 2011).

At the aforementioned overburden stress conditions and assuming isotropy: (1) the weight of the overlying geological materials above elevation z corresponds to $\sigma_v = g\int_z^{z_t} \rho_r(u)\,du$, where ρ_r is the wet density of the granular material at a given elevation, and z_t is the top (surface) elevation and (2) λ depends only on the Poisson's ratio: $\lambda = \nu/(1-\nu)$.

At the regional scale, the deformation of an aquifer system is essentially vertical. The value of horizontal strains is much lower, and may be difficult to detect. However, at the local scale, the horizontal strains may be large, such as close to an abrupt inflection of the basement topography (Galloway and Burbey 2011). Despite this, in regional analysis, it is reasonable to neglect horizontal deformation. Moreover, assuming (1) the vertical deformation is exclusively driven by the change in porosity due to the shifting of incompressible solid grains, as well as the closure of intergranular voids and (2) the validity of the law of elasticity for small strains, yields:

$$d\varepsilon_v = \frac{dV}{V} = \frac{d\phi}{(1-\phi)} = -\frac{1}{E}d\sigma' \qquad (2)$$

where ε_v is the vertical deformation, V is the bulk volume, ϕ is the porosity, and E is the formation vertical elasticity coefficient under fully saturated conditions (reciprocal of the vertical compressibility coefficient).

From Equation 2, it follows that at no effective stress (at ground level) the porosity is ϕ_0 and that under effective stress σ' the porosity is ϕ. Integrating Equation 2 under these conditions yields:

$$\int_{\phi_0}^{\phi} \frac{d\phi}{(1-\phi)} = -\frac{1}{E}\int_0^{\sigma'} d\sigma'$$

$$\sigma' = E\ln\left(\frac{1-\phi}{1-\phi_0}\right) \qquad (3)$$

Following this method, a zero-effective porosity ($\phi \approx 0$) occurs when the applied effective stress is:

$$\sigma'_0 = -E\ln(1-\phi_0) \qquad (4)$$

where σ'_0 denotes the limit stress for pore closure. Expressing Equation 4 for the formation elasticity E, and introducing it into Equation 3, yields:

$$\sigma' = \frac{-\sigma'_0}{\ln(1-\phi_0)}\ln(1-\phi) + \sigma'_0$$
$$= \sigma'_0\left(1 - \frac{\ln(1-\phi)}{\ln(1-\phi_0)}\right) \qquad (5)$$

and an effective stress-dependent porosity is obtained by expressing Equation 5 as:

$$\phi\left(\sigma'\right) = 1 - (1-\phi_0)^{\left(1-\frac{\sigma'}{\sigma'_0}\right)} \tag{6}$$

A negative effective stress results in a porosity greater than the no-stress porosity: $\phi \geq \phi_0$. This can be interpreted as water pressure bearing all the applied loads, so that grains are no longer in contact with each other, but suspended in the fluid (soil boiling phenomenon).

Hydraulic Conductivity and Specific Storage Coefficient

As expressed by the Kozeny-Carman equation (Kozeny 1927; Carman 1937), the hydraulic conductivity of granular porous media depends on the dynamic properties of water and on the intrinsic properties of the granular material:

$$K = \frac{\rho_w g}{\mu_w} \frac{\phi^3}{b A_s^2} \tag{7}$$

where μ_w is the water viscosity, b is a factor taking into account the shape and spatial arrangement of grains (in general: $10 < b < 30$, usually $b \approx 20$), and A_s is the specific contact area, defined as (Cornaton and Perrochet 2006):

$$A_s = 3(1-\phi) C = \frac{3 (1-\phi)}{R_h} \tag{8}$$

where the coefficient C corresponds to the inverse of the harmonic mean radius of grains in the sample, R_h:

$$C = \frac{1}{R_h} = \int_0^\infty \frac{P(r)}{r} \mathrm{d}r \tag{9}$$

In Equation 9, the symbol r stands for the grain radius, and $P(r)$ is the frequency distribution: $P(r) = 1/P_0 \; \partial P_{cum}/\partial r$, where P_{cum} is the cumulative weight and P_0 is the total weight of the formation sample. For a soil with uniformly distributed grain size with minimum radius r_1 and maximum radius r_2, that is, $P(r) = 1/(r_2 - r_1)$, Equation 9 yields:

$$C = \int_{r_1}^{r_2} \frac{1}{r_2 - r_1} \frac{\mathrm{d}r}{r} = \frac{1}{r_2 - r_1} \ln\left(\frac{r_2}{r_1}\right) \tag{10}$$

Table 1 presents some values of C calculated from sample particle size distribution curves.

Assuming that at large scale, the coefficient C is constant, that is, it does not change despite the shifting of incompressible solid grains, and introducing Equation 6 into Equation 7 results in an effective stress-dependent hydraulic conductivity:

Table 1
Typical Ranges of Coefficient C for Granular Geological Materials

Geological Material	C (1/m)
Pebble gravel stream channel	~1000
Sandy gravel	~3500
Fine sand	~7000
Alluvial sandy gravel	~13,500
Sandy-silty gravel moraine	~36,000
Silty sand	~36,500
Lacustrine clayey silt	~205,500

$$K\left(\sigma'\right) = \frac{\rho_w g}{\mu_w} \frac{1}{9} \frac{\left(1 - (1-\phi_0)^{\left(1-\frac{\sigma'}{\sigma'_0}\right)}\right)^3}{\left((1-\phi_0)^{\left(1-\frac{\sigma'}{\sigma'_0}\right)} C\right)^2 b} \tag{11}$$

Similarly, Equation 6 can be inserted in the definition of the specific storage coefficient, S_s:

$$S_s\left(\sigma'\right) = \rho_w g \left(\frac{1}{E_s} + \frac{\phi}{E_w}\right) \tag{12}$$

$$S_s\left(\sigma'\right) = \rho_w g \left(\frac{1}{E_s} + \frac{1 - (1-\phi_0)^{\left(1-\frac{\sigma'}{\sigma'_0}\right)}}{E_w}\right) \tag{13}$$

where E_w and E_s stand for the bulk modulus of elasticity of water and the skeletal elasticity, respectively. If water is assumed incompressible, the skeletal elasticity E_s corresponds to the formation elasticity under fully saturated conditions E.

Using Equations 11 and 13 results in a nonlinear effective stress-dependent groundwater flow equation:

$$S_s\left(\sigma'\right) \frac{\partial H}{\partial t} = \nabla \cdot \left(K\left(\sigma'\right) \nabla H\right); \quad H = h + z \tag{14}$$

where H is hydraulic head and t is time. Knowledge of ϕ_0, E, C, and b is sufficient to solve Equation 14 under any given boundary conditions.

Deformation

From Equation 6, it follows that a change in effective stress causes a change in porosity $\Delta\phi$:

$$\Delta\phi = \phi\left(\sigma'_i\right) - \phi\left(\sigma'\right) = (1-\phi_0)^{\left(1-\frac{\sigma'}{\sigma'_0}\right)} - (1-\phi_0)^{\left(1-\frac{\sigma'_i}{\sigma'_0}\right)} \tag{15}$$

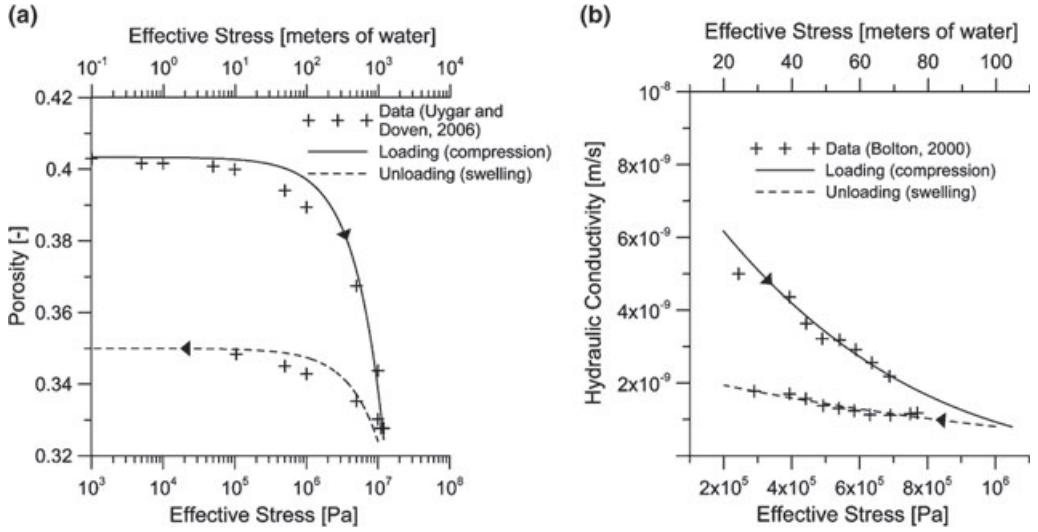

Figure 2. Fitting example of Equations 6 and 11 on laboratory stress-dependent data for (a) an uniformly graded fine sand from Uygar and Doven (2006) and (b) an artificial silty clay from Bolton (2000). Cross symbols are measured data and lines are simulated values for loading (solid line) and unloading (dashed line).

where the subscript i denotes the effective stress state prior to the change. $\Delta\phi$ is positive in consolidation and negative in expansion. Integrating vertically over all the porosity changes from the bottom z_b to the top z_t leads to the system consolidation $T > 0$ or expansion $T < 0$:

$$T(x, y) = \int_{z_b}^{z_t} \Delta\phi(x, y, z) \, dz \tag{16}$$

Parameter Estimation by Fitting the Measured Data

Parameter values (ϕ_0, σ'_0, and C) can be obtained by fitting Equation 6 or Equation 11 to measured field or laboratory data.

Uygar and Doven (2006) studied the porosity response of a uniformly graded fine sand at saturated, drained conditions under cyclic high effective stresses. Bolton (2000) investigated the hydraulic conductivity of artificial silty clay during a loading and unloading test. Fitting of Equations 6 and 11 on the measured data of Uygar and Doven (2006) and Bolton (2000) is presented in Figure 2 for a loading (compression) and unloading (expansion) cycle. The unique calibrated parameters are presented in Table 2.

From the data of Figure 2, it follows that applied virgin compression results in a nonelastic irreversible deformation, changing the mechanical and hydraulic characteristics of the granular porous media.

Modeling Approach

This modeling approach allows regional simulation of changes in the vertical volume of the porous medium in response to changes in fluid pressure, that is, a hydromechanical fluid-to-solid interaction (Rutqvist and Stephansson 2003; Bundschuh and Arriaga 2010). Principal stresses are assumed to be constants, and shear stresses are neglected. Thus, only the change in water pressure affects the effective stress tensor. The method consists of three simulation phases.

Simulation of Overburden Stress

The principal overburden stresses of the stress tensor $\boldsymbol{\sigma}$ in Equation 1, characterizing the stress state of a sedimentary basin filled with unconsolidated sediments can be rapidly and easily calculated for a two-dimensional (2D) or 3D domain Ω by the following boundary value problem:

$$\nabla \cdot \frac{1}{\rho_r(x, y, z)} \mathbf{N} \nabla\sigma = 0 \ \text{ in } \Omega,$$
$$\mathbf{N} = \nabla z \otimes \nabla z = \begin{bmatrix} 0 & 0 & 0 \\ 0 & 0 & 0 \\ 0 & 0 & 1 \end{bmatrix} \tag{17}$$
$$\sigma(z_{surface}) = f_1(x, y, z_{surface}, t) \ \text{ on } \Gamma_+$$
$$\mathbf{N} \nabla\sigma \cdot \mathbf{n} = \frac{d\sigma}{dz} = -g\rho_{rbottom} \ \text{ on } \Gamma_-$$

where f_1 is a known function detailing the magnitude of the overburden stress at the upper boundary Γ_+ (topographic surface). Set to zero and constant over time, this Dirichlet boundary condition indicates that there are no weights applied on the surface (heavy buildings, civil engineering structures or water bodies). The Neumann condition on the bottom boundary Γ_- corresponds to the wet density of the bottom geological material $\rho_{rbottom}$ multiplied by the gravitational acceleration. $\mathbf{N}$ is a singular 3D tensor with vertical anisotropy and $\mathbf{n}$ is the unit normal vector.

Table 2
Numerical Values Used for the Curve Fitting of Figure 2.

	ϕ_0 (–)	σ'_0 (Pa)	E (Pa)	C (1/m)	b (–)
Uygar and Doven (2006)					
Loading	0.40	50.0×10^6	96.8×10^6	—	—
Unloading	0.35	110.0×10^6	255.3×10^6	—	—
Bolton (2000)					
Loading	0.40	2.0×10^6	3.9×10^6	10^6	20
Unloading	0.29	3.5×10^6	10.2×10^6	10^6	20

In a finite-element scheme, solving Equation 17 results in the definition of the overburden vertical stress $\sigma_{zz} = \sigma_v$:

$$\sigma_{zz}(x, y, z) = g \int_z^{z_t} \rho_r(x, y, u)\ \mathrm{d}u \tag{18}$$

Finally, considering the Poisson's ratio effect results in the horizontal principal stresses $\sigma_h = \sigma_{xx} = \sigma_{yy}$:

$$\sigma_h = \lambda \sigma_v; \quad \lambda = \frac{\nu}{1 - \nu} \tag{19}$$

Simulation of Flow

The transient effective stress-dependent groundwater flow equation, Equation 14, is used to model the distribution of hydraulic head, pressure head, and discharge and recharge rates of the aquifer system. The problem is nonlinear, because pressure heads (water pressures) are considered with overburden stresses for the calculation of effective stresses, on which depend the hydrodynamic parameters of Equation 14.

Simulation of Aquifer Deformation

The aquifer system deformation resulting from a change in the effective stress state is subsequently simulated using Equations 15 and 16, with the effective stress distributions obtained from the flow simulation as input. For the 2D or 3D domain this problem can be solved as follows:

$$\nabla \cdot \mathbf{N} \nabla T = \frac{\mathrm{d}\Delta\phi}{\mathrm{d}z} \ \text{in}\,\Omega \tag{20}$$

$$T(x, y, z_{\text{bottom}}) = 0 \ \text{on}\,\Gamma_-$$

$$\mathbf{N} \nabla T \cdot \mathbf{n} = 0 \ \text{on}\,\Gamma_+$$

where the bottom boundary condition specifies that the aquifer consolidation or expansion is zero at the system base, and the upper boundary condition states that at the surface, there is no change in porosity.

This three-step modeling approach allows rapid (not-computationally demanding) analysis of regional basins affected by important changes in water pressure. The governing equations require only five parameters (ρ_r, ϕ_0, E, C, and b), to capture the essence of the physical process.

Illustrative Simulation and Verification

Pumping

An illustrative simulation represents vertical deformation of a regional aquifer system due to heavy groundwater pumping. Initial and boundary conditions are based on the compaction problem of Leake and Hsieh (1997), and the illustrative modeling domain is inspired by the geometry of the Mexico City Basin.

An impervious and incompressible basement is faulted, creating a basin. This geometry is filled by four sedimentary layers: a stratum of unconsolidated volcanic deposits overlaid by alluvial sediments constituting a thick and compressible lower aquifer, a layer of lacustrine sediments forming a semiconfining and highly compressible unit, and an upper alluvial aquifer. The 3D virtual basin geometry is obtained by full rotation of the cross section shown in Figure 3.

The upper aquifer is under a constant hydraulic head matching the topographic elevation of 2300 m.a.s.l. Heavy pumping in the center of the lower aquifer decreases the hydraulic head at a rate of 12 m/year until reaching a final hydraulic head of 1300 m.a.s.l. (Figure 3). The system is initially at hydrostatic conditions, 2300 m.a.s.l.

The simulation is run for a period of 100 years using (1) the approach presented in this paper and (2) the poroelasticity theory of Biot (1941). The boundary conditions for the poroelastic computation are those of the Leake and Hsieh's (1997) problem. With poroelastic equations, the model is run only on the 2D basin cross section because of the aforementioned computational problems of this method in regional 3D analysis. With the proposed approach, the model is run on the 3D basin. Within the direction of rotation, this virtual basin is isotropic. Of course, this is geologically unlikely, but this allows to (1) test the proposed approach on a 3D model and (2) compare its results with detailed poroelastic data. The approach discussed in this paper was implemented in the multipurpose Ground Water (GW) finite element software (Cornaton 2007). The multiphysics software COMSOL Multiphysics (2010) was used to solve poroelastic equations. Parametric information is presented in Table 3.

Discussion and Results

Using effective stress-dependent parameters in the groundwater flow equation, Equation 14, results in

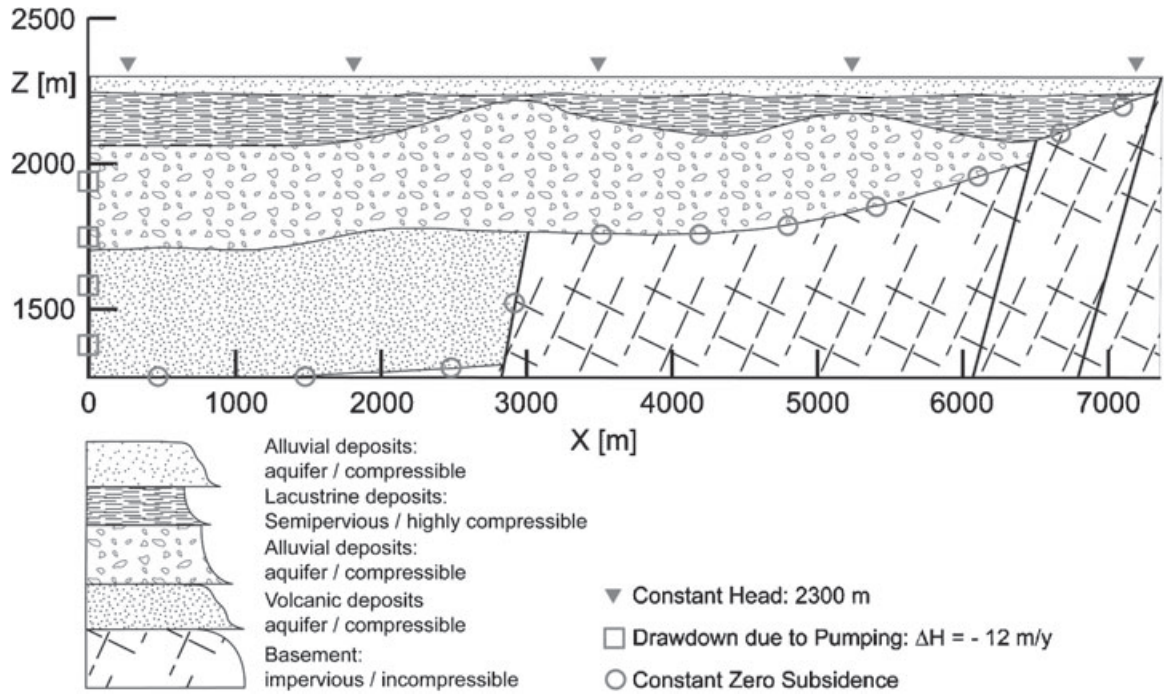

Figure 3. Cross section of the regional model geometry and boundary conditions. The left boundary corresponds to the basin center and the right boundary to the external limits (vertical exaggeration 2×).

Table 3
Parameter Values Used in the Pumping Simulation

Approach Presented in This Paper								
Lithology	ρ_r (kg/m^3)	ϕ_0 (−)	σ'_0 (MPa)	E (GPa)	C (1/m)	b (−)	K_0 (m/s)	S_{S_0} (1/m)
Upper alluvial	1800	0.23	286	1.1	1000	20	10^{-3}	10^{-5}
Lacustrine deposits	1800	0.50	70	0.1	158,100	20	10^{-6}	10^{-4}
Lower alluvial	2000	0.37	464	1.0	2500	20	10^{-3}	1.1×10^{-4}
Volcanic deposits	2200	0.12	62	0.5	1000	20	10^{-4}	2.0×10^{-5}
Poroelasticity Theory								
Lithology	ρ_r (kg/m^3)	ϕ (−)	E_Y (GPa)	ν (−)	α_B (−)	K (m/s)		
Upper alluvial	1800	0.23	11	0.25	1	10^{-3}		
Lacustrine deposits	1800	0.50	1	0.25	1	10^{-6}		
Lower alluvial	2000	0.37	10	0.25	1	10^{-3}		
Volcanic deposits	2200	0.12	5	0.25	1	10^{-4}		
Fluid and Other Parameters								
ρ_w (kg/m^3)	μ_w (Pa s)		E_w (GPa)			g (m/s^2)		
1000	10^{-3}		2.5			9.81		

Note that for the proposed approach σ'_0, K_0, and S_{s_0} are calculated via ϕ_0, E, C, and b using Equations 4, 11, and 13.

increased hydraulic gradients (Figure 4b) and in decreased simulated pumping rates (Figure 4c) compared with the linear form with constant parameters. This is because of the reduction in hydraulic conductivity and specific storage due to the decrease in water pressure and increase in effective stress. The overburden stress field used in the flow simulation obtained using Equation 17 is constant (Figure 4a).

The simplified approach presented in this paper generally reproduces the vertical deformation obtained

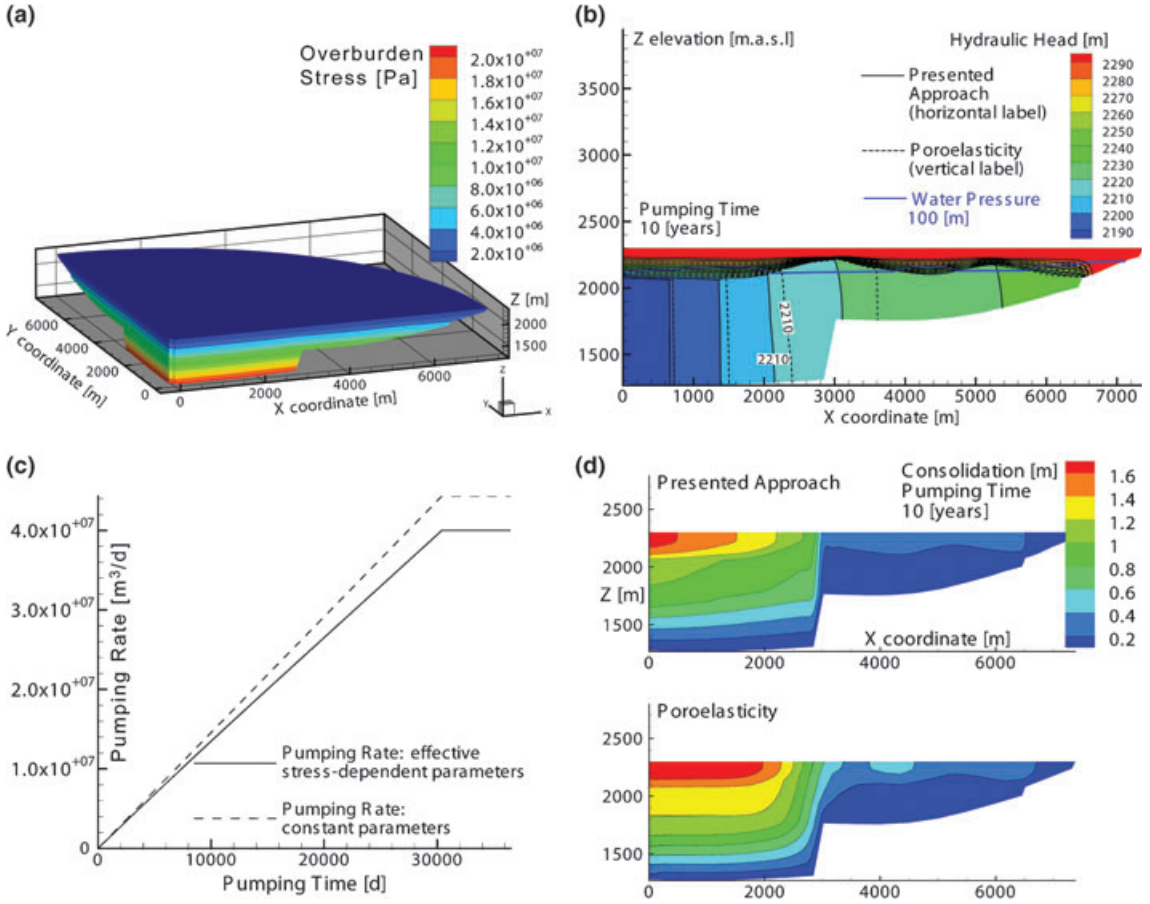

Figure 4. (a) Three dimensional view of a quarter of the basin showing the simulated overburden stress. (b) Simulated hydraulic head field at 10 years of pumping with the presented approach (solid black lines) and with poroelasticity (dashed lines), the solid blue line is the isocontour of 100 m of water pressure calculated with the presented approach. (c) Pumping rate divergence considering constant (dashed line) or variable (solid line) hydrodynamic parameters. (d) Aquifer system consolidation at 10 years of pumping. Top: method illustrated in this paper; bottom: Biot's poroelasticity theory.

using the detailed poroelastic equations (Figure 4d). However, the consolidation is less pronounced. This is because the decline in water pressure is slowed by the parameter dependency. Note that: (1) in Table 3, E_Y denotes the Young's modulus of the porous medium and (2) poroelasticity theory does not use specific storage but rather uses Young's modulus and Poisson's ratio (Leake and Hsieh 1997).

Differential ground settlement due to bedrock inflection is correctly highlighted by the proposed modeling approach. These areas can be subject to ground failure.

Recovery of Porosity

After 100 years pumping stops, and due to the upper boundary condition, the aquifer system gradually returns to the initial hydrostatic situation. Here we compare porosity recovery using the proposed approach and the three cases illustrated in Figure 5a: (1) the aquifer system has an elastic behavior, (2) only aquifer units are elastic, and (3) the system has an inelastic behavior.

Discussion and Results

In the case of full elasticity, porosity recovery and media expansion are the same as the change in porosity and the compaction induced by the 100 years of pumping. If stress due to pumping causes nonrecoverable deformations, the expansion curve is different than the compression curve (Figure 5a), and there is an important loss in porosity (and permeability), and only a fraction of the ground subsidence can be recovered, especially if all formations have inelastic behavior (Figure 5b).

No change and recovery in porosity occurs in the upper aquifer, due to constant water pressure. Not surprisingly, in the inelastic case, considerable loss of porosity occurs in the lacustrine aquitard unit. However, the strongest decrease in porosity occurs in the deeper aquifer, where the increase in effective stresses during pumping caused significant nonrecoverable deformations.

Laboratory consolidation tests (Bolton 2000; Uygar and Doven 2006; Galloway and Burbey 2011) and field observations (Helm 1975) indicate that inelasticity must be considered when studying aquifer system deformation due to changing water pressure. Equations 6, and 11 can be used, after a fitting on laboratory consolidation tests, for first estimates of the recoverable porosity of regional aquifer systems affected by induced stresses such as heavy pumping.

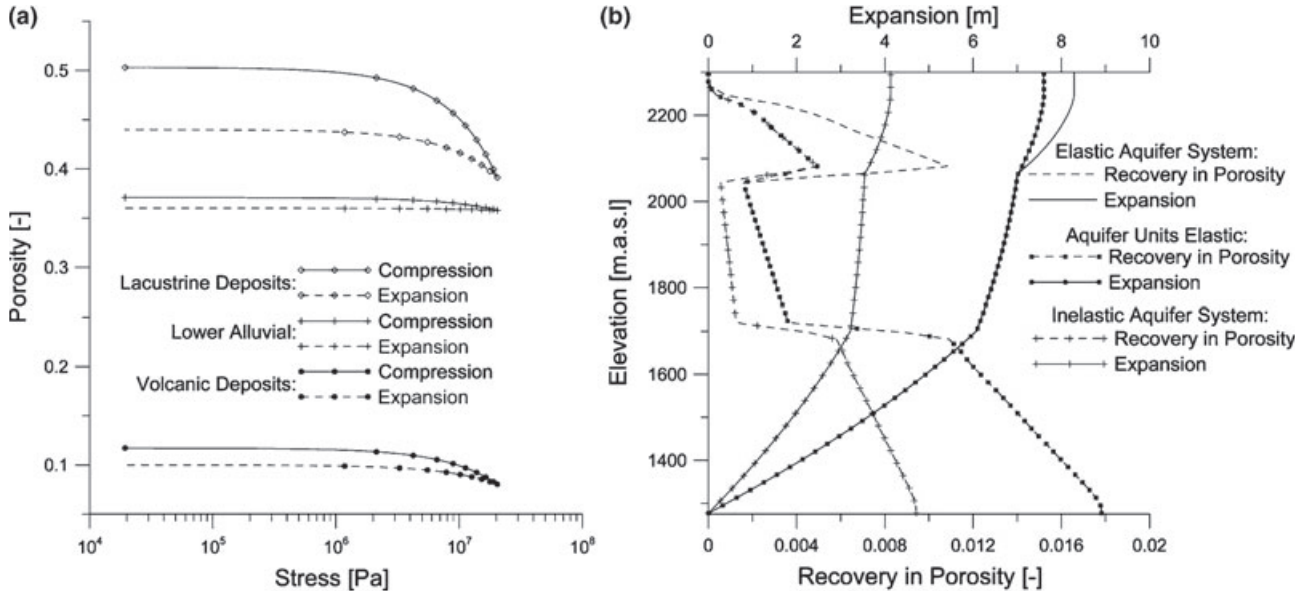

Figure 5. (a) Effective stress-dependent porosity functions used in the recovery analysis. Solid lines illustrate compression due to pumping and dashed lines illustrate expansion during recovery. (b) Simulated recovery in porosity (dashed lines) and expansion (solid lines) as a function of elevation. Note that curves of change in porosity and consolidation due to 100 years of groundwater pumping match curves of recovery in porosity and expansion for an elastic aquifer system.

Conclusion

Hydrodynamic parameters depend on effective stresses in regional basin-fill aquifer systems. Effective stress-dependent equations for porosity, hydraulic conductivity, and specific storage have been developed based on the law of elasticity. These equations correctly reproduce the data obtained in stress-porosity/hydraulic conductivity laboratory tests.

The paper has also presented a computationally simple approach to simulating the dynamics of regional aquifer systems affected by significant changes in water pressure. In this approach, the groundwater flow equation becomes physically more accurate because it considers the aforementioned relationships. The simple deformation equations based on the change in porosity due to the variation in water pressures require only five unknown parameters to reproduce vertical deformation similar to that obtained by detailed poroelastic equations.

The presented approach is limited by the following assumptions: (1) the stress field is constant with water pressure variations, and (2) horizontal displacements and (3) deformation within solid grains are negligible. However, each of these assumptions are reasonable for most regional hydrogeological problems, so that the proposed approach can be a simple and rapid tool for estimating the dynamics of aquifer systems affected by change in water pressures.

Acknowledgments

The authors wish to thank Prof. Philip Brunner for his constructive comments and Jessica Meeks for her revision of English, and are particularly grateful to the anonymous reviewers for their constructive comments, as well as the improvement of English.

Notation

A_s	Specific contact area, (1/m)
b	Factor taking into account the shape and spatial arrangement of grains, (m)
C	Coefficient describing the inverse of the harmonic mean radius of grains in a sample, (1/m)
E	Formation elasticity coefficient under fully saturated conditions, (Pa)
E_s	Skeletal elasticity: reciprocal of skeletal compressibility $\alpha_s = 1/E_s$, (Pa)
E_w	Bulk modulus of elasticity of water: reciprocal of water compressibility $\beta_w = 1/E_w$, (Pa)
E_Y	Young's modulus of the porous medium, (Pa)
g	Gravitational acceleration, (m/s^2)
h	Pressure head, (m)
H	Hydraulic head, (m)
$\mathbf{n}$	Unit normal vector, (–)
$\mathbf{N}$	Singular 3D tensor with vertical anisotropy, (–)
p	Water pressure, (Pa)
$P(r)$	Frequency distribution of grains radius, (–)
r	Grain radius, (m)
R_h	Harmonic mean radius of grains in a sample, (m)
S_s	Specific storage coefficient, (1/m)

S_{s_0}	Specific storage coefficient at no stress, (1/m)
t	Time, (s)
T	Aquifer system consolidation ($T > 0$) or expansion ($T < 0$), (m)
V	Bulk volume, (m^3)
x, y	Spatial coordinates, (m)
z	Elevation head, spatial coordinate, (m)
$\boldsymbol{\alpha_B}$	Biot-Willis coefficient tensor, (–)
$\Delta\phi$	Change in porosity, (–)
ε_v	Vertical deformation, (–)
K	Hydraulic conductivity, (m/s)
K_0	Hydraulic conductivity at no stress, (m/s)
λ	Ratio of horizontal to vertical stress, (–)
μ_w	Water viscosity, (Pa s)
ν	Poisson's ratio, (–)
ρ_w, ρ_r	Water density, wet density of the granular material, (kg/m^3)
$\boldsymbol{\sigma}$	Stress tensor, (Pa)
σ_h, σ_v	Horizontal, vertical stress, (Pa)
$\boldsymbol{\sigma}'$	Effective stress tensor, (Pa)
σ'_0	Limit effective stress for pore closure, (Pa)
ϕ, ϕ_0	Porosity, porosity at no stress, (–)

References

Bell, J., F. Amelung, A. Ferretti, M. Bianchi, and F. Novali. 2008. Permanent scatterer InSAR reveals seasonal and long-term aquifer system response to groundwater pumping and artificial recharge. *Water Resources Research* 44, no. 2: W02407.

Biot, M. 1941. General theory of three-dimensional consolidation. *Journal of Applied Physics* 12, no. 2: 155–164.

Bolton, A. 2000. Some measurements of permeability and effective stress on a heterogeneous soil mixture: implications for recovery of inelastic strains. *Engineering Geology* 65, no. 1–2: 95–104.

Bundschuh, J., and M. Arriaga. 2010. Rock and fluid. In *Introduction to the Numerical Modeling of Groundwater and Geothermal Systems*, 13–100. London, UK: Taylor & Francis Group, CRC Press.

Carman, P.C. 1937. Fluid flow through granular bed. *Transactions of the Institution of Chemical Engineers (London)* 15: 150–156.

COMSOL Multiphysics. 2010. *COMSOL Multiphysics User's Guide*. Sweden: COMSOL AB.

Cornaton, F.J. 2007. *Ground Water: A 3D Ground Water and Surface Water Flow, Mass Transport and Heat Transfer Finite Element Simulator. Reference Manual*. Neuchâtel, Switzerland: Centre for Hydrogeology and Geothermics.

Cornaton, F.J., and P. Perrochet. 2006. Groundwater age, life expectancy and transit time distributions in advective-dispersive systems: 2. Reservoir theory for sub-drainage basins. *Advances in Water Resources* 29, no. 9: 1292–1305.

Detournay, E., and A.H.D. Cheng. 1993. Fundamentals of poroelasticity. In *Comprehensive Rock Engineering: Principles, Practice and Projects*, Vol. II, ed. C. Fairhurst, 113–171. Oxford – New York: Pergamon Press.

Ferronato, M., G. Gambolati, C. Janna, and P. Teatini. 2010. Geomechanical issues of anthropogenic CO_2 sequestration in exploited gas fields. *Energy Conversion and Management* 51, no. 10: 1918–1928.

Galloway, D., and T.J. Burbey. 2011. Review: Regional land subsidence accompanying groundwater extraction. *Hydrogeology Journal* 19, no. 8: 1459–1486.

Gambolati, G., P. Teatini, and M. Ferronato. 2005. Anthropogenic land subsidence. In *Encyclopedia of Hydrological Sciences*, ed. M.G. Anderson, 17. Chichester: John Wiley & Sons.

Gangi, A.F. 1978. Variation of whole and fractured porous rock permeability with confining pressure. *International Journal of Rock Mechanics and Mining Sciences and Geomechanics Abstracts*, 15, 5: 249–257.

Hansmann, J., S. Loew, and K. Evans. 2012. Annual opening and closure of alpine valleys. *Hydrogeology Journal* 20, no. 1: 73–91.

Helm, D. 1976. One-dimensional simulation of aquifer system compaction near pixley, California. 2. Stress-dependent parameters. *Water Resources Research* 12, no. 3: 375–391.

Helm, D. 1975. One-dimensional simulation of aquifer system compaction near Pixley, California. 1. Constant parameters. *Water Resources Research* 11, no. 3: 465–478.

Helm, D. 1972. Simulation of aquitard compaction due to changes in stress. *Transactions, American Geophysical Union* 53, no. 11: 979.

Holzer, T. 1984. *Man Induced Land Subsidence*. Washington, DC: Geol Soc of America.

Jacob, C. 1950. Flow and ground water. In *Engineering hydraulics: Proceedings of the Fourth Hydraulics Conference*, ed. H. Rouse. Iowa City, Iowa: Iowa Institute of Hydraulic Research.

Jacob, C. 1940. On the flow of water in an elastic artesian aquifer. *American Geophysical Union* 21: 574–586.

Kihm, J., J.M. Kim, S. Song, and G. Lee. 2007. Three-dimensional numerical simulation of fully coupled groundwater flow and land deformation due to groundwater pumping in an unsaturated fluvial aquifer system. *Journal of Hydrology* 335, no. 1–2: 1–14.

Kim, J.M. 2005. Three-dimensional numerical simulation of fully coupled groundwater flow and land deformation in unsaturated true anisotropic aquifers due to groundwater pumping. *Water Resources Research* 41, no. 1: 16.

Kim, J.M., and R. Parizek. 1999. A mathematical model for the hydraulic properties of deforming porous media. *Ground Water* 37, no. 4: 546–554.

Kozeny, J. 1927. Ueber kapillare Leitung des Wassers im Boden. *Tech Rep 2a, Akad Wiss Wien, AUT*.

Leake, S., and P. Hsieh. 1997. Simulation of deformation of sediments from decline of ground-water levels in an aquifer underlain by a bedrock step. USGS Technical Report 97-47. Reston, Virginia: USGS.

Lombardi, G. 1988. Les tassements exceptionnels au barrage de Zeuzier. *Publication de la Société Suisse de Mécanique des Sols et des Roches* 118, no. 1: 39–47.

Louis, C. 1969. A study of groundwater flow in jointed rock and its influence on the stability of rock masses. Technical Report 9, Rock Mechanics. London, UK: Imperial College.

Murdoch, L.C., and L.N. Germanovich. 2006. Analysis of a deformable fracture in permeable material. *International Journal for Numerical and Analytical Methods in Geomechanics* 30, no. 6: 529–561.

National Research Council. 1996. *Rock fractures and fluid flow*. Washington, DC: National Academy Press.

Parriaux, A. 2006. *Géologie: Bases pour l'Ingénieur*. Lausanne: Presses Polytechniques et Universitaires Romandes.

Price, D., and M. de Freitas. 2009. *Engineering Geology*. Berlin/Heidelberg: Springer.

Rutqvist, J., Y.S. Wu, C.F. Tsang, and G. Bodvarsson. 2002. A modeling approach for analysis of coupled multiphase fluid flow, heat transfer, and deformation in fractured porous rock. *International Journal of Rock Mechanics and Mining Sciences* 39, no. 4: 429–442.

Rutqvist, J., and O. Stephansson. 2003. The role of hydromechanical coupling in fractured rock engineering. *Hydrogeology Journal* 11, no. 1: 7–40.

Terzaghi, K. 1923. Die Berechnung der Durchlässigkeitziffer des Tones aus dem Verlauf der hydrodynamischen Spannungserscheinungen. *Akad Wissensch Wien Sitzungsber Mathnaturwissensch Klasse IIa* 142, no. 3–4: 125–138.

Terzaghi, K., and R. Peck. 1967. *Soil Mechanics in Engineering Practice*. New York: John Wiley and Sons Inc.

Uygar, E., and A. Doven. 2006. Monotonic and cyclic oedometer tests on sand at high stress levels. *Granular Matter* 8, no. 1: 19–26.

Verruijt, A. 2008. Consolidation of soils. In *Encyclopedia of Hydrological Sciences*, ed. M.G. Anderson, 15. Chichester: John Wiley & Sons.

Walsh, J.B. 1981. Effect of pore pressure and confining pressure on fracture permeability. *International Journal of Rock Mechanics and Mining Sciences & Geomechanics Abstracts* 18, no. 5: 429–435.

Zangerl, C., E. Eberhardt, and S. Loew. 2003. Ground settlements above tunnels in fractured crystalline rock: Numerical analysis of coupled hydromechanical mechanisms. *Hydrogeology Journal* 11, no. 1: 162–173.